

Flattened Hall response from coherent dynamics of topological phase transition and Weyl semimetals

Yong Xu^{1*} and Ying Hu^{2,3}

¹ Center for Quantum Information, IIIS, Tsinghua University, Beijing 100084, PR China

² State Key Laboratory of Quantum Optics and Quantum Optics Devices,
Institute of Laser Spectroscopy, Shanxi University, Taiyuan, Shanxi 030006, China and

³ Collaborative Innovation Center of Extreme Optics,
Shanxi University, Taiyuan, Shanxi 030006, China

Recent experimental realization of synthetic topological models in ultracold atomic gases have stimulated extensive studies on dynamics of topological systems when a Hamiltonian is varied across distinct topological phases. However, previous study shows that the coherent dynamics of Hall response exhibits strong and long-lasting oscillations even for slow variation of a system parameter due to the non-adiabatic passage through a gap closing point. Here we demonstrate that the Hall response can coherently follow the change of the Chern number of a Hamiltonian without oscillations, owing to the electric field induced damping, thus paves the way for observing the topological phase transition through measuring the intrinsic physical quantity of the Hall response. Furthermore, high controllability of ultracold atomic gases allows for implementation and manipulation of simple Weyl semimetals. We find that tuning a parameter in a Hamiltonian of Weyl semimetals, combined with appropriate manipulation of an electric field, enables us to control the corresponding Hall response without oscillations, despite the existence of a gapless band structure. Our finding lays the theoretical foundation for observation and tuning of Weyl semimetals in ultracold atomic gases.

High and versatile controllability of ultracold atomic gases allows for observation of quantum phase transition, such as superfluid-Mott insulator transition [1, 2], through slow variation of Hamiltonian parameters. Further, recent realizations of the topological Haldane model [3, 4] and spin-orbit-coupled Chern insulator [5, 6] in ultracold atomic gases provide an ideal platform to study the topological phase transition in dynamics of a system under either slow or rapid variation of Hamiltonian parameters [7–26]. In this context, one important and fundamental question is whether the intrinsic observable, anomalous quantum Hall conductivity, conventionally viewed as the order parameter for a static Chern insulator, follows the change of a Hamiltonian through a topological phase transition by slowly varying a parameter. However, in coherent dynamics, the Chern number of the many-body wavefunction of the system cannot change even though the topology of a Hamiltonian changes [7, 8]. Further research reveals that the non-equilibrium Hall response exhibits strong and long-lasting oscillations [27–29] even for the slow ramp of Hamiltonian parameters due to the inevitable non-adiabatic transitions through the gap closing point. In this work, we will show that these oscillations can be eliminated, leading to a remarkable flattened and asymptotically quantized Hall response from coherent dynamics through the topological phase transition (see Fig. 1).

The above issue also arises in the context of three-dimensional (3D) Weyl semimetals [30], which have seen a rapid development in a variety of fields [31–52]. Weyl semimetals feature *gapless* band structures characterized by the existence of pairs of Weyl points, which can be regarded as the topological phase transition points between

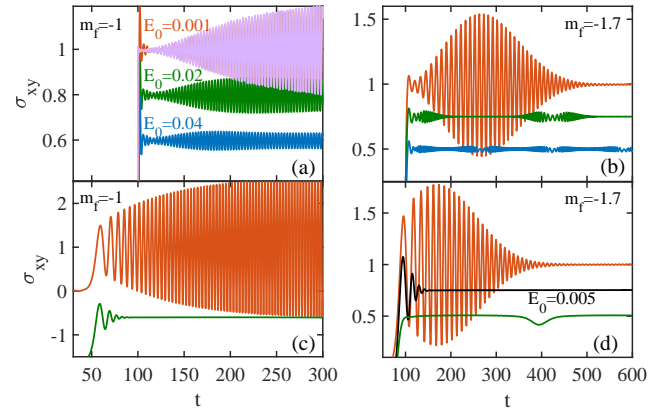


FIG. 1. (Color online) Coherent dynamics of the Hall response for various strength of electric field in two different protocols (see main text). Panels in the upper (lower) row correspond to the first (second) protocol. Here $m_i = -2.5$, $v = 0.02$ and $\tau_e = 10$. For visibility, we have shifted the Hall response downward for different E_0 . All curves are computed by the exact numerical method except for the pink curve in panel (a), which is calculated based on the perturbation approach.

the topologically trivial and nontrivial insulators in momentum space. As a consequence, Weyl semimetals in their ground state are known to exhibit topological Hall response [33, 34], which is not quantized, but rather determined by the location and the number of Weyl points. In cold atom setups, creation and manipulation of Weyl points can be achieved through the time-modulation of Hamiltonian parameters [40, 49, 50]. However, due to the aforementioned topological constraint, the instantaneous many-body wavefunction itself cannot be used to signal the dynamical variations of Weyl points. In view

of the dynamical Hall response, on the other hand, a main difficulty stems from the fact that, due to the gapless character of Weyl semimetal, the system will undergo non-adiabatic time evolution at all times, rendering important irregularities in coherent dynamics of response functions, regardless of how slow the Hamiltonian parameter can be tuned.

In this work, we demonstrate that a *flattened* non-equilibrium Hall response manifesting the topological property of the *instantaneous* Hamiltonian can smoothly build up in *coherent dynamics*, despite topologically trivial time-evolved state. We show this for a non-equilibrium Chern insulator, where the system parameter is slowly ramped from the topologically trivial to nontrivial regimes, thus driving the Hamiltonian through a phase transition at the gap closing point. We find that the realization of a smooth topological non-equilibrium Hall response relies on three elements: (i) whether the electric field is turned on before or after the gap closing point, (ii) the strength of electric field as compared to the ramp velocity, and (iii) the dispersion of the band structure of the final Hamiltonian. We further show this smooth Hall response for a non-equilibrium Weyl semimetal as pairs of Weyl points are created and their separation is continuously tuned by means of slow modifications of Hamiltonian parameters. Our findings thus provide the theoretical foundation for experimentally observing and controlling Weyl points in ultracold atomic gases.

We start by considering a Chern insulator in the $x - y$ plane, motivated by its recent realization with ultracold atoms using Raman laser beams [6]. The relevant time dependent Hamiltonian is $H[m_z(t)] = \sum_{\mathbf{k}} c_{\mathbf{k}}^\dagger H[\mathbf{k}, m_z(t)] c_{\mathbf{k}}$ where

$$H[\mathbf{k}, m_z(t)] = \mathbf{d}_{\mathbf{k}}(t) \cdot \boldsymbol{\sigma} \quad (1)$$

with $d_x = \sin(k_x)$, $d_y = \sin(k_y)$, $d_z = m_z(t) + \cos(k_x) + \cos(k_y)$ at lattice momentum $\mathbf{k} = (k_x, k_y)$, and $\boldsymbol{\sigma} = (\sigma_x, \sigma_y, \sigma_z)$ are the Pauli matrices. Here the energy is measured in units of hopping amplitude. In the cold-atom experiment, the mass parameter m_z arises from the two-photon detuning and can be controlled. For static m_z , the ground state of Hamiltonian is in the topological nontrivial phase with Chern number $C = -\text{sgn}(m_z)$ for $-2 < m_z < 2$, otherwise, it is in the topological trivial phase with $C = 0$.

We will be interested in the coherent dynamics of Hall response in an experimental relevant scenario, where the system is initially prepared in the topologically trivial ground state of Hamiltonian $H(m_i)$ with $m_i < -2$. We tune m_z slowly from m_i to $-2 < m_f < 0$ according to $m_z(t) = m_i + (m_f - m_i)(1 - e^{-vt})$ with velocity v . This way, Hamiltonian $H[m_z(t)]$ changes its topology from trivial to topologically nontrivial, undergoing a transition at an energy gap closing point at critical time t_c . To probe Hall response, at time t_e , we ramp on an electric field in the x direction as $E_x(t) = E_0(1 - e^{-t/\tau_e})$,

which in experiments of cold atoms can be generated via a homogeneous time-dependent synthetic gauge field, i.e., $E_x(t) = \partial_t A(t)$. The Hall current in the y direction is computed by

$$J_y(t) = \frac{1}{2\pi} \int_{\text{BZ}} d\mathbf{k} \langle \psi_{\mathbf{k}}(t) | \partial_{k_y} H[\mathbf{k}'(t), m_z(t)] | \psi_{\mathbf{k}}(t) \rangle, \quad (2)$$

where $|\psi_{\mathbf{k}}(t)\rangle$ denotes the instantaneous wavefunction at momentum \mathbf{k} , and the integration is over the first Brillouin zone (BZ). Note that the presence of electric field induces a shift in momentum via $\mathbf{k}'(t) = [k_x + A(t), k_y]$. The non-equilibrium Hall response is thus $\sigma_{xy}(t) = J_y(t)/E_x(t)$, measured in unit of e^2/h .

We will analyze and compare the coherent dynamics of Hall response in two different protocols for controlling the electric field: (1) We first vary the mass parameter without electric field $E_x(t)$. Then, some time after the transition of system through the critical point at time t_c , the $E_x(t)$ is turned on, i.e., $t_e \gg t_c$. (2) The $E_x(t)$ is turned on before the modulations of m_z , i.e., $t_e \ll t_c$. The numerical results for the coherent dynamics of Hall response in both protocols are shown in Fig. 1.

We find that, while a Hall response dynamically builds up after the Hamiltonian is ramped into a topological nontrivial regime, its equilibration to a topologically quantized value under coherent evolution crucially depends on two elements for both protocols: (i) dispersion of the energy band of the final Hamiltonian $H(m_f)$ and (ii) the magnitude of E_0 . In more details, for $m_f = -1$ [Fig. 1 (a) and (c)], where the corresponding energy band is flat along k_x for $k_y = 0$, we see that the non-equilibrium Hall response exhibits strong and persistent oscillations for $E_0 \ll v$ in both protocols [see red curves for $E_0 = 0.001$], as also found earlier [27, 28]. Remarkably, when E_0 is increased to be comparable to the ramp velocity [e.g., see green curves for $E_0 = 0.02$], such irregularities disappear after a few oscillations in protocol (2), as opposed to its counterpart in protocol (1) where the oscillations are only moderately suppressed. When the underlying energy band becomes increasingly dispersive, such as for $m_f = -1.7$ [Figs. 1 (b), (d)], we see that the oscillations of the Hall response generically damps out at long times even for weak E_0 in both protocols, and increasing E_0 can significantly reduce the time for stabilization. These findings show that a smooth and asymptotically quantized non-equilibrium Hall response can build up from coherent dynamics, despite the non-adiabatic passage through the gap closing.

To gain insight into above dynamical behavior of Hall response, we first analyze protocol (1) using the perturbation approach. In this case, the energy gap closes at lattice momentum $\mathbf{k}_c = (0, 0)$ at time t_c . Then at time t_e when $E_x(t)$ is turned on, for simplicity and to capture the essential physics, we assume that $H(m_f)$ has been reached and the state can be described by $|\psi_{\mathbf{k}}(t_e)\rangle = \sqrt{1 - p(\mathbf{k})} e^{iD_1(\mathbf{k})} |u_-(\mathbf{k})\rangle + e^{i\theta(\mathbf{k})} e^{-iD_1(\mathbf{k})} \sqrt{p(\mathbf{k})} |u_+(\mathbf{k})\rangle$

for $\mathbf{k} \neq 0$, where $|u_{+(-)}(\mathbf{k})\rangle$ denotes the excited (ground) state of $H(\mathbf{k}, m_f)$, $\theta(\mathbf{k})$ is the relative phase, and $D_1(\mathbf{k}) = \int_0^{t_e} \epsilon_+(\mathbf{k}, m_z(t')) dt'$ is the dynamical phase with $\epsilon_{+(-)}(\mathbf{k}, m_z(t))$ the eigenenergy of Hamiltonian $H(\mathbf{k}, m_z(t))$. Moreover, $p(\mathbf{k})$ denotes the number of excitations created during the non-adiabatic passage through the gap closing. At times $t > t_e$, where the gap has been reopened, using time-dependent perturbation theory [53], the evolution of $|u_\lambda(\mathbf{k})\rangle$ can be approximated by $(\hbar \equiv 1) |\Phi_\lambda(\mathbf{k}', t)\rangle = e^{-i \int_{t_e}^t \epsilon_\lambda(\mathbf{k}') dt'} e^{i \gamma_\lambda(t)} \times \left[|u_\lambda(\mathbf{k}')\rangle - i E_0 \frac{\langle u_\lambda(\mathbf{k}') | \partial_{k_x} | u_\lambda(\mathbf{k}') \rangle}{2 \lambda \epsilon_+(\mathbf{k}')} |u_{\bar{\lambda}}(\mathbf{k}')\rangle \right]$ with $\mathbf{k}' = [k_x + A(t), k_y]$. Here $\bar{\lambda} \neq \lambda$ and $\gamma_\lambda(t)$ is associated with the Berry phase in the λ band. Therefore, after ramping on the electric field, the state evolves from $|\psi_{\mathbf{k}}(t_e)\rangle$ into: $|\psi_{\mathbf{k}}(t > t_e)\rangle = \sqrt{1 - p(\mathbf{k})} e^{i D_1(\mathbf{k})} |\Phi_-(\mathbf{k}', t)\rangle + e^{i \theta(\mathbf{k})} e^{-i D_1(\mathbf{k})} \sqrt{p(\mathbf{k})} |\Phi_+(\mathbf{k}', t)\rangle$. Substitution of this ansatz into Eq. (2) then gives the non-equilibrium Hall current, which well captures the dynamical behavior of Hall response at times $t > t_e$, as evidenced by the pink curve in Fig. 1(a).

The non-equilibrium Hall current thus contains three contributions, i.e.,

$$J_y(t) = J_{\text{Hall}}(t) + J_{\text{Dis}}(t) + J_{\text{Osc}}(t). \quad (3)$$

Here, $J_{\text{Hall}}(t) = (E_0/2\pi) \int_{\text{BZ}} d\mathbf{k} [p(\mathbf{k}) \Omega_+(\mathbf{k}') + (1 - p(\mathbf{k})) \Omega_-(\mathbf{k}')]]$ describes the weighted anomalous Hall current which has topological origin, with Ω_\pm labeling the instantaneous Berry curvature for the upper (lower) band of $H(\mathbf{k}', m_f)$. In the limit of vanishing ramp velocity, $J_{\text{Hall}}(t)/E_0$ approaches the Chern number of $H(m_f)$. The current $J_{\text{Dis}} = (1/2\pi) \int_{\text{BZ}} d\mathbf{k} [p(\mathbf{k}) \partial_{k_y} \epsilon_+(\mathbf{k}') + (1 - p(\mathbf{k})) \partial_{k_y} \epsilon_-(\mathbf{k}')]]$ arises from the weighted band velocity, which exactly vanishes because of the underlying symmetry in our system, i.e., $\epsilon_\lambda(k_x, k_y) = \epsilon_\lambda(k_x, -k_y)$. The current $J_{\text{Osc}}(t)$ comes from the coherent superpositions between the upper and lower bands, i.e.,

$$J_{\text{Osc}}(t) = \text{Re} \int_{\text{BZ}} d\mathbf{k} \sqrt{p_k(1 - p_k)} e^{i[\theta(\mathbf{k}) - D_2(\mathbf{k}')] } \Gamma(t), \quad (4)$$

where $D_2(\mathbf{k}') = 2 \int_{t_e}^t dt' \epsilon_+(\mathbf{k}')$ and $\Gamma(t) = \frac{1}{\pi} e^{-2i D_1(\mathbf{k})} e^{i(\gamma_+ - \gamma_-)} \left[g_{12} - 2i E_0 h_{12} \frac{\partial_{k_y} \epsilon_+(\mathbf{k}', m_f)}{2 \epsilon_+(\mathbf{k}', m_f)} \right]$ with $g_{12}(\mathbf{k}') = \langle u_-(\mathbf{k}') | \partial_{k_y} H(\mathbf{k}', m_f) | u_+(\mathbf{k}') \rangle$, and $h_{12} = \langle \partial_{k_x} u_-(\mathbf{k}') | u_+(\mathbf{k}') \rangle$. Obviously, $J_{\text{Osc}}(t)$ is responsible for the oscillation as we detail below.

Equation (4) allows us to understand the effect of electric field on the oscillations and their damping in the coherent dynamics of Hall response as shown in Figs. 1(a) and (b). In our analysis we will focus on the term involving g_{12} while ignoring that involves h_{12} , which is small due to gapped energy as is numerically verified. For a slow ramp, the excitations occur in a very narrow region near the gap-closing point at $\mathbf{k}_c = (0, 0)$, which can be described in the context of Landau-Zener (LZ) physics that

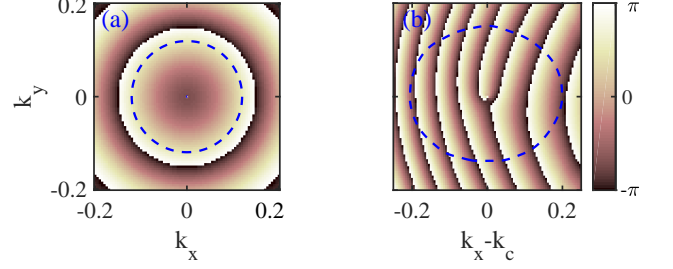


FIG. 2. (Color online) Profiles of $\theta(\mathbf{k})$ near the gap closing point \mathbf{k}_c (for $\mathbf{k} \neq \mathbf{k}_c$) in the $k_x - k_y$ plane for (a) protocol (1) with $k_c = 0$ and (b) protocol (2) with $k_c = -A(t_c)$ and $E_0 = 0.02$. At lattice momenta depicted by the dashed blue line, the corresponding population in the excited state is 0.1.

gives $p(\mathbf{k}) \approx e^{-\pi k^2 / v_{\text{LZ}}}$, with $v_{\text{LZ}} = (m_f + 2)v$. Hence the dominant contribution to $J_{\text{Osc}}(t)$ comes from the lattice momenta $|\mathbf{k}| < \sqrt{v_{\text{LZ}}/\pi}$. In this regime, in the limit of weak electric field $E_0 \rightarrow 0$, one can expand g_{12} in terms of A on the time scale $t \ll (\sqrt{v_{\text{LZ}}/\pi})/E_0$, and the main contribution to $J_{\text{Osc}}(t)$ comes from the first term, i.e., $g_{12} \propto A = E_0(t - t_e)$. Therefore, for sufficiently weak electric field such as in $E_0 = 0.001$, the amplitude of oscillating Hall response will always undergo an initial increase with time, as shown in Figs. 1(a) and (b).

In the long time limit when $\sqrt{v_{\text{LZ}}/\pi} \ll A(t) < 2\pi/E_0$, which is quickly fulfilled as in the case when $E_0 = 0.02$, we find that the oscillations persist for $m_f = -1$ while can be damped out for $m_f \neq -1$ as shown in Figs. 1(a) and (b). The damping is caused by the significant difference for the energy spectrum $\epsilon_+(\mathbf{k}')$ along the k_x direction, which is strongly modified by the presence of large $A(t)$. To gain some intuitive understanding, let us keep only the dominant term responsible for the strong damping, $D_2(\mathbf{k}')$, and approximate $J_{\text{Osc}}(t)$ by $J_{\text{Osc}}(t) \sim 2 \text{Re} \int d\mathbf{k} \sqrt{p_k(1 - p_k)} e^{2i \epsilon_-(\mathbf{k} + \mathbf{k}_e, m_f) t'}$ with $t' = t - t_e$, where we have taken the leading term $g_{12} \approx 1$ and ignored the time independent phase contribution and the Berry phase, which is irrelevant due to its small variation in momentum space. To see the effect of spectrum difference, let us fix \mathbf{k}_e (which is driven by the electric field by $k_{ex} = E_0 t$), e.g., $k_{ex} = \pi/2$, where dispersion exhibits the largest derivative along k_x for $k_y = 0$ and $|m_f| \neq 1$. We find that the oscillations decays exponentially for $m_f = -1.5$ and $v = 0.02$. However, when $m_f = -1$, we find $J_{\text{Osc}} \sim \sqrt{ct'}/(1 - ict')$ with $c = 2v_{\text{LZ}}/\pi$ in the long time limit, which decays very slowly, almost leading to a persistent oscillation, consistent with Fig. 1(a), because of flat energy dispersion for $k_y = 0$. Further, the oscillations of Hall currents revive as it approaches a period of $2\pi/E_0$ because Bloch oscillation occurs [see blue curve in Fig. 1(b)]. This also implies that the coherent oscillations of Hall currents cannot be completely damped out if the relevant time for damping $> \pi/E_0$.

Above analysis guides our intuition into the remark-

ably smooth Hall response in protocol (2). As $E_x(t)$ is present initially before $m_z(t)$ is varied, the energy gap closing point is shifted to $\mathbf{k}_c = [-A(t_c), 0]$. This motivates us to consider the form of Eq. (4) with the replacement $p(\mathbf{k}) \rightarrow p(\mathbf{k} + \mathbf{k}_c)$ and $\theta(\mathbf{k}) \rightarrow \theta(\mathbf{k} + \mathbf{k}_c)$. For $E_x \rightarrow 0$, such shift remains sufficiently small. Thus the oscillating dynamics of Hall response in protocol (2) is expected to exhibit similar behavior as the counterpart in protocol (1) [see red curves Figs. (1)(c)]. However, when $E_0 = 0.02$, we find that $\theta(\mathbf{k} + \mathbf{k}_c)$ exhibits rapid variations near \mathbf{k}_c along the x direction [see Fig. 2(b) calculated by the exact numerical method], in sharp contrast to the counterpart of protocol (1) [see Fig. 2(a)], where $\theta(\mathbf{k})$ varies slowly. The rapid variations introduce the strong damping as the integration over momentum space is performed, leading to a remarkably smooth Hall response in protocol (2) reflecting the topology of the instantaneous Hamiltonian, even for $m_f = -1$.

Finally, it is interesting to extend our analysis to three dimensional (3D) Weyl semimetals, which can exhibit anomalous Hall effects. We consider a system of atoms in a 3D lattice described by the Hamiltonian (see SM for realization scheme)

$$H_C = \frac{\mathbf{p}^2}{2m} - \sum_{\nu=x,y,z} V_\nu \cos^2(k_{L\nu} r_\nu) + m_z \sigma_z + V_{\text{SO}}. \quad (5)$$

Here m is the mass of atoms, \mathbf{p} is the momentum operator, $V_{\text{SO}} = M_y \sigma_x - M_x \sigma_y$ describes the nondiagonal optical lattices with $M_x = \Omega_{\text{SO}} \sin(k_{Lx} r_x) \cos(k_{Ly} r_y) \cos(k_{Lz} r_z)$ and $M_y = \Omega_{\text{SO}} \sin(k_{Ly} r_y) \cos(k_{Lx} r_x) \cos(k_{Lz} r_z)$. Further, the diagonal lattice potential in direction ν is characterized by the strength $V_\nu > 0$ and the period $a_\nu = \pi/k_{L\nu}$. Hamiltonian (5) can be recast into the following tight-binding form (see SM for derivation), i.e., $H_{\text{TB}} = \sum_{\mathbf{x}} [-\sum_{\nu} (J_\nu \hat{c}_{\mathbf{x}}^\dagger \hat{c}_{\mathbf{x}+a_\nu \mathbf{e}_\nu} + \text{H.c.}) + m_z \hat{c}_{\mathbf{x}}^\dagger \sigma_z \hat{c}_{\mathbf{x}} + (-1)^{j_x+j_y+j_z} J_{\text{SO}} (\hat{c}_{\mathbf{x}}^\dagger \sigma_y \hat{c}_{\mathbf{x}+a_x \mathbf{e}_x} - \hat{c}_{\mathbf{x}}^\dagger \sigma_x \hat{c}_{\mathbf{x}+a_y \mathbf{e}_y} + \text{H.c.})]$. Here $\hat{c}_{\mathbf{x}}^\dagger = \begin{pmatrix} \hat{c}_{\mathbf{x}\uparrow}^\dagger & \hat{c}_{\mathbf{x}\downarrow}^\dagger \end{pmatrix}$ with $\hat{c}_{\mathbf{x}\sigma}$ ($\hat{c}_{\mathbf{x}\sigma}^\dagger$) annihilating (creating) an atom with spin σ at $\mathbf{x} = \sum_{\nu} j_\nu a_\nu \mathbf{e}_\nu$. The corresponding Bloch Hamiltonian at lattice momentum $\mathbf{k} = (k_x, k_y, k_z)$ can be written as

$$H_{3\text{D}}(\mathbf{k}) = m_z \sigma_z - h_t \tau_x + \tau_y (d_y \sigma_x - d_x \sigma_y), \quad (6)$$

where τ_ν denotes the Pauli matrix describing the sublattices, $h_t = -2 \sum_{\nu=x,y,z} J_\nu \cos(k_\nu a_\nu)$, $d_x = 2J_{\text{SO}} \sin(k_x a_x)$ and $d_y = 2J_{\text{SO}} \sin(k_y a_y)$. The eigenenergy corresponding to Hamiltonian (6) is $E_\pm(\lambda) = \pm \sqrt{d_x^2 + d_y^2 + (h_t - \lambda m_z)^2}$ with $\lambda = \pm 1$. Below we will assume $J_\nu = J$ for convenience.

The semimetal (6) exhibits a very rich phase diagram. When $|m_z| > 6J$, the Weyl semimetal is in the trivial insulating phase. When $2J < |m_z| < 6J$, the system is in the topological phase featuring one pair of Weyl points, whereas for $|m_z| < 2J$ and $m_z \neq 0$, the semimetal has

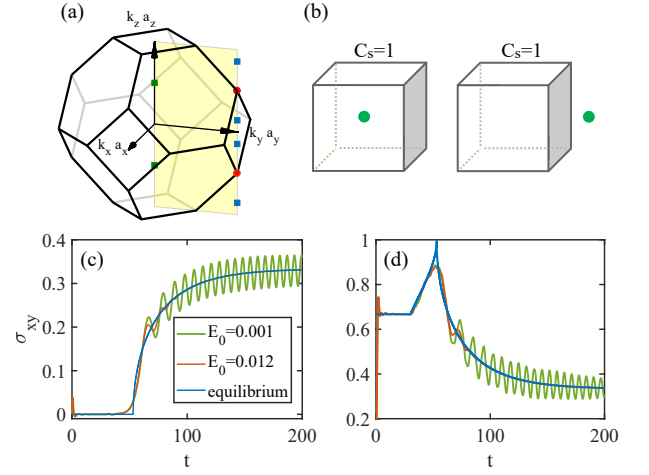


FIG. 3. (Color online) (a) The first Brillouin zone with a pair of Dirac points, one and two pairs of Weyl points, denoted by the solid red circles, green and blue squares, respectively. (b) Schematics illustrating that the Chern number of states remains unchanged on a closed surface when a Weyl point moves out of the surface. Evolution of the Hall response over time as m_z varies slowly (c) from $-7J$ to $-5J$ and (d) from $-3J$ to $-J$. Here the unit of time is \hbar/J .

two pairs of Weyl points. For $m_z = 0$, the system is the Dirac semimetal with two Dirac points [54]. The locations of Weyl points and Dirac points in momentum space are displayed in Fig. 3(a). If we choose a closed surface enclosing a Weyl point as shown in Fig. 3(b), we find that the Chern number of states on the surface remains unchanged over time even if the Weyl point moves out of the surface, implying the Chern number of states does not reflect the Chern number of the Hamiltonian.

In Figs. 3(c) and (d), we show the coherent dynamics of Hall response in the y direction for the considered Weyl semimetal [55], when an electric field $E_x(t)$ is switched on before $m_z(t)$ is slowly tuned. Importantly, we see that the non-equilibrium Hall response at $E_0 = 0.012$ is finally stabilized to the value of its equilibrium counterpart dictated by the instantaneous Hamiltonian as we slowly tune the system from a topological trivial insulator to a Weyl semimetal phase with two Weyl points (see Fig. 3(c)) and from a phase with two Weyl points to another phase with four points (see Fig. 3(d)); this is in sharp contrast to the case for $E_x = 0.001$ where the Hall response exhibits strong oscillations, as we have discussed earlier.

In summary, we have studied the non-equilibrium Hall response by slowly tuning a 2D system from a topological trivial to nontrivial phase in a coherent manner. We find that the Hall response can approach a quantized value of the Chern number of the final Hamiltonian, in stark contrast to previous results with strong oscillations, implying that the intrinsic topological property can signal the topological phase transition from coherent dynamics as observed in equilibrium case. It is important to note

that the damping is driven by the electric field instead of involving any effects of environment such as engineering the noise [27]. Furthermore, we propose a simple Weyl semimetal model and explore their Hall response to an electric field as a parameter in the Hamiltonian is tuned. We find that the Hall response approaches the value dictated by the final Hamiltonian in equilibrium, provided a moderately strong electric field is applied. Our findings pave the way for observation and controlling of Weyl semimetals in ultracold atomic gases.

We thank D.-L. Deng, Y.-K. Wu and Z.-X. Gong for helpful discussions. Y. X. is supported by Tsinghua start up program and National Thousand-Young-Talents Program. Y. H. acknowledges support from the National Thousand-Young-Talents Program, the National Key Research and Development Program of China (Grant Nos. 2016YFA0301700, 2017YFA0304203), and Changjiang Scholars and Innovative Research Team in University of Ministry of Education of China (Grant No. IRT13076)

* yongxuphy@tsinghua.edu.cn

- [1] M. Greiner, O. Mandel, T. Esslinger, T. W. Hänsch, and I. Bloch, *Nature (London)* **415**, 39, (2002).
- [2] M. Greiner, O. Mandel, T. W. Hänsch, and I. Bloch, *Nature (London)* **419**, 51, (2002).
- [3] G. Jotzu, M. Messer, R. Desbuquois, M. Lebrat, T. Uehlinger, D. Greif, and T. Esslinger, *Nature (London)* **515**, 237 (2014).
- [4] N. Fläschner, B. Rem, M. Tarnowski, D. Vogel, D.-S. Lühmann, K. Sengstock, and C. Weitenberg, *Science* **352**, 1091 (2016).
- [5] Z. Wu, L. Zhang, W. Sun, X.-T. Xu, B.-Z. Wang, S.-C. Ji, Y. Deng, S. Chen, X.-J. Liu, and J.-W. Pan, *Science*, **354**, 83 (2016).
- [6] W. Sun, B.-Z. Wang, X.-T. Xu, C.-R. Yi, L. Zhang, Z. Wu, Y. Deng, X.-J. Liu, S. Chen, and J.-W. Pan, [arXiv:1710.00717](https://arxiv.org/abs/1710.00717) (2017).
- [7] L. D'Alessio and M. Rigol, *Nat. Commun.* **6**, 8336 (2015).
- [8] M. D. Caio, N. R. Cooper, and M. J. Bhaseen, *Phys. Rev. Lett.* **115**, 236403 (2015).
- [9] J. C. Budich and M. Heyl, *Phys. Rev. B* **93**, 085416 (2016).
- [10] P. Wang, M. Schmitt, and S. Kehrein, *Phys. Rev. B* **93**, 085134 (2016).
- [11] J. H. Wilson, J. C.W. Song, and G. Refael, *Phys. Rev. Lett.* **117**, 235302 (2016).
- [12] M. D. Caio, N. R. Cooper, and M. J. Bhaseen, *Phys. Rev. B* **94**, 155104 (2016).
- [13] F. N. Ünal, E. J. Mueller, and M. Ö. Oktel, *Phys. Rev. A* **94**, 053604 (2016).
- [14] C. Wang, P. Zhang, X. Chen, J. Yu, and H. Zhai, *Phys. Rev. Lett.* **118**, 185701 (2017).
- [15] Y. Ge and M. Rigol, *Phys. Rev. A* **96**, 023610 (2017).
- [16] C. Yang, L. Li, and S. Chen, *Phys. Rev. B* **97**, 060304 (2018).
- [17] M. Tarnowski, F. N. Ünal, N. Fläschner, B. S. Rem, A. Eckardt, K. Sengstock, and C. Weitenberg, [arXiv:1709.01046](https://arxiv.org/abs/1709.01046) (2017).
- [18] M. Heyl and J. C. Budich, *Phys. Rev. B* **96**, 180304(R) (2017).
- [19] M. Schüler and P. Werner, *Phys. Rev. B* **96**, 155122 (2017).
- [20] A. Kruckenhauser and J. C. Budich, [arXiv:1712.02440](https://arxiv.org/abs/1712.02440) (2017).
- [21] N. Fläschner, D. Vogel, M. Tarnowski, B. S. Rem, D.-S. Lühmann, M. Heyl, J. C. Budich, L. Mathey, K. Sengstock, and C. Weitenberg, *Nat. Phys.* **14**, 265 (2018).
- [22] W. Sun, C.-R. Yi, B.-Z. Wang, W.-W. Zhang, B. C. Sanders, X.-T. Xu, Z.-Y. Wang, J. Schmiedmayer, Y. Deng, X.-J. Liu, S. Chen, and J.-W. Pan, [arXiv:1804.08226](https://arxiv.org/abs/1804.08226) (2018).
- [23] L. Zhang, L. Zhang, S. Niu, and X.-J. Liu, [arXiv:1802.10061](https://arxiv.org/abs/1802.10061) (2018).
- [24] J. Yu, [arXiv:1804.10358](https://arxiv.org/abs/1804.10358) (2018).
- [25] Z. Gong and M. Ueda, [arXiv:1710.05289](https://arxiv.org/abs/1710.05289) (2018).
- [26] X. Qiu, T.-S. Deng, G.-C. Guo, and W. Yi, [arXiv:1804.09032](https://arxiv.org/abs/1804.09032) (2018).
- [27] Y. Hu, P. Zoller, and J. C. Budich, *Phys. Rev. Lett.* **117**, 126803 (2016).
- [28] A. Dauphin, D.-T. Tran, M. Lewenstein, and N. Goldman, *2D Materials*, **4**, 024010 (2017).
- [29] L. P. Gavensky, G. Usaj, and C. A. Balseiro, [arXiv:1806.04733](https://arxiv.org/abs/1806.04733) (2018).
- [30] N. P. Armitage, E. J. Mele, and A. Vishwanath, *Rev. Mod. Phys.* **90**, 015001 (2018).
- [31] G. E. Volovik, *The Universe in a Helium Droplet* (Clarendon Press, Oxford, 2003).
- [32] X. Wan, A. M. Turner, A. Vishwanath, and S. Y. Savrasov, *Phys. Rev. B* **83**, 205101 (2011).
- [33] K.-Y. Yang, Y.-M. Lu, and Y. Ran, *Phys. Rev. B* **84**, 075129 (2011).
- [34] A. A. Burkov and L. Balents, *Phys. Rev. Lett.* **107**, 127205 (2011).
- [35] G. Xu, H. Weng, Z. Wang, X. Dai, and Z. Fang, *Phys. Rev. Lett.* **107**, 186806 (2011).
- [36] M. Gong, S. Tewari, and C. Zhang, *Phys. Rev. Lett.* **107**, 195303 (2011).
- [37] L. Lu, L. Fu, J. D. Joannopoulos, and M. Soljačić, *Nat. photon.* **7**, 294 (2013).
- [38] Y. Xu, R.-L. Chu, and C. Zhang, *Phys. Rev. Lett.* **112**, 136402, (2014).
- [39] S. A. Yang, H. Pan, and F. Zhang, *Phys. Rev. Lett.* **113**, 046401 (2014).
- [40] T. Dubček, C. J. Kennedy, L. Lu, W. Ketterle, M. Soljačić, and H. Buljan, *Phys. Rev. Lett.* **114**, 225301 (2015).
- [41] B. Liu, X. Li, L. Yin, and W. V. Liu, *Phys. Rev. Lett.* **114**, 045302 (2015).
- [42] H. Weng, C. Fang, Z. Fang, B. A. Bernevig, and X. Dai, *Phys. Rev. X* **5**, 011029 (2015).
- [43] S.-Y. Xu, I. Belopolski, N. Alidoust, M. Neupane, C. Zhang, R. Sankar, S.-M. Huang, C.-C. Lee, G. Chang, B. Wang, G. Bian, H. Zheng, D. S. Sanchez, F. Chou, H. Lin, S. Jia, and M. Z. Hasan, *Science* **349**, 613 (2015).
- [44] B. Q. Lv, H. M. Weng, B. B. Fu, X. P. Wang, H. Miao, J. Ma, P. Richard, X. C. Huang, L. X. Zhao, G. F. Chen, Z. Fang, X. Dai, T. Qian, and H. Ding, *Phys. Rev. X* **5**, 031013 (2015).
- [45] L. Lu, Z. Wang, D. Ye, L. Ran, L. Fu, J. D. Joannopoulos, and M. Soljačić, *Science* **349**, 622 (2015).
- [46] X. Li and S.D. Sarma, *Nat. Commun.* **6**, 7137 (2015).
- [47] Y. Xu, F. Zhang, and C. Zhang, *Phys. Rev. Lett.* **115**,

- 265304 (2015).
 [48] H. Ishizuka, T. Hayata, M. Ueda, and N. Nagaosa, Phys. Rev. Lett. **117**, 216601 (2016).
 [49] W.-Y. He, S. Zhang, and K. T. Law, Phys. Rev. A **94**, 013606 (2016).
 [50] Y. Xu and L.-M. Duan, Phys. Rev. A **94**, 053619 (2016).
 [51] Z. Yan and Z. Wang, Phys. Rev. Lett. **117**, 087402 (2016).
 [52] H. Hübener, M. A. Sentef, U. D. Giovannini, A. F. Kemper, and A. Rubio, Nat. Commun. **8**, 13940 (2017).

- [53] D. Xiao, M.-C. Chang, and Q. Niu, Rev. Mod. Phys. **82**, 1959 (2010).
 [54] The Dirac points can be clearly seen from the transformed Hamiltonian in a partitioned diagonal form: $H(\mathbf{k}) = \tau_z [-h_t \sigma_z + d_x \sigma_x + d_y \sigma_y] + m_z \sigma_z \tau_0$.
 [55] For simplicity, we perform a transformation $\hat{a}_{\mathbf{x}\uparrow} = (-1)^{j_x+j_y+j_z} \hat{c}_{\mathbf{x}\uparrow}$ and $\hat{a}_{\mathbf{x}\downarrow} = \hat{c}_{\mathbf{x}\downarrow}$, giving a simpler Hamiltonian in momentum space, $H'_{3D}(\mathbf{k}) = (-h_t + m_z) \sigma_z + d_x \sigma_x + d_y \sigma_y$, which has the same form as the 2D Hamiltonian (1), regarding k_z as a parameter.

SUPPLEMENTAL MATERIAL

In the supplemental material, we will provide the details for calculation of the phases $\theta(\mathbf{k} + \mathbf{k}_c)$ induced by the electric field and propose an experimental scheme for realization of a Weyl semimetal described by the continuous model in Eq. (5) in the main text and derive its tight-binding Hamiltonian.

First, to calculate the phase $\theta(\mathbf{k} + \mathbf{k}_c)$ induced by the electric field, we expand the state in the basis of instantaneous eigenstates $|u_\lambda(\mathbf{k}', m_z(t))\rangle$ as

$$|\psi_{\mathbf{k}}(t)\rangle = \sum_{\lambda=\pm} \alpha_\lambda(\mathbf{k}, t) A_\lambda(\mathbf{k}, t) |u_\lambda(\mathbf{k}', m_z(t))\rangle, \quad (\text{S1})$$

where $|u_\lambda(\mathbf{k}', m_z(t))\rangle$ satisfies $H(\mathbf{k}', m_z(t))|u_\lambda(\mathbf{k}', m_z(t))\rangle = \epsilon_\lambda(\mathbf{k}', m_z(t))|u_\lambda(\mathbf{k}', m_z(t))\rangle$ with $\epsilon_\lambda(\mathbf{k}', m_z(t)) = \lambda \sqrt{\sum_{\nu=x,y,z} d_\nu^2(\mathbf{k}', m_z(t))}$ and $\lambda = \pm 1$, $A_\lambda(\mathbf{k}, t) = e^{-i \int_0^t \epsilon_\lambda(\mathbf{k}', m_z(t')) dt'} e^{i \gamma_\lambda(t)}$ corresponding to the dynamical and Berry phases $\gamma_\lambda(t) = i \int_0^t dt' \langle u_\lambda(\mathbf{k}', m_z(t')) | \partial_{t'} u_\lambda(\mathbf{k}', m_z(t')) \rangle$, respectively. Plugging Eq. (S1) into the Schrödinger equation yields

$$\partial_t \alpha_- = -f(t) \alpha_+ A_+ / A_-, \quad (\text{S2})$$

$$\partial_t \alpha_+ = f(t)^* \alpha_- A_- / A_+, \quad (\text{S3})$$

where $f(t) = \langle u_-(\mathbf{k}, m_z(t)) | \partial_t u_+(\mathbf{k}, m_z(t)) \rangle$. Supposing that all atoms are initialized to the lower band, we can calculate the time evolution of $\alpha_\lambda(\mathbf{k}, t)$, obtaining $\theta(\mathbf{k}) = \text{angle}(\alpha_+(\mathbf{k}, t > t_c) / \alpha_-(\mathbf{k}, t > t_c))$.

Second, to implement the continuous model in Eq. (5) in the main text, we only need to slightly revise our previous scheme for realization of a 4D dynamical Weyl nodal ring [S1]. We refer the reader to Figs. (3)(c-d) for a laser configuration setup, where two sets of Raman laser beams are utilized to generate the off-diagonal spin-dependent optical lattices. Each set includes two pairs of Raman laser beams. In the first set, for one pair, the Rabi frequencies are: $[\bar{\Omega}_1 = -\bar{\Omega}_{10} \cos(k_{Ly} r_y) e^{-ik_{Lz} r_z / 2}, \bar{\Omega}_2 = i\bar{\Omega}_{20} \sin(k_{Lx} r_x) e^{ik_{Lz} r_z / 2}]$, and for the other pair, they are $[\bar{\Omega}'_1 = -\bar{\Omega}_{10} \cos(k_{Ly} r_y) e^{ik_{Lz} r_z / 2}, \bar{\Omega}'_2 = i\bar{\Omega}_{20} \sin(k_{Lx} r_x) e^{-ik_{Lz} r_z / 2}]$. In the second set, for one pair, the Rabi frequencies are: $[\tilde{\Omega}_1 = \tilde{\Omega}_{10} \sin(k_{Ly} r_y) e^{-ik_{Lz} r_z / 2}, \tilde{\Omega}_2 = \tilde{\Omega}_{10} \cos(k_{Lx} r_x) e^{ik_{Lz} r_z / 2}]$, and for the other pair, they are $[\tilde{\Omega}'_1 = \tilde{\Omega}_{10} \sin(k_{Ly} r_y) e^{ik_{Lz} r_z / 2}, \tilde{\Omega}'_2 = \tilde{\Omega}_{10} \cos(k_{Lx} r_x) e^{-ik_{Lz} r_z / 2}]$. We also require another laser beam to create an optical lattice along z . Using this scheme, we can achieve the Hamiltonian in Eq. (7).

To obtain the continuous model's tight-binding Hamiltonian, let us write down the many-body Hamiltonian using the field operator

$$H_{II} = \int d\mathbf{r} \hat{\psi}^\dagger(\mathbf{r}) H_C \hat{\psi}(\mathbf{r}), \quad (\text{S4})$$

where $\hat{\psi}(\mathbf{r}) = [\hat{\psi}_\uparrow(\mathbf{r}) \ \hat{\psi}_\downarrow(\mathbf{r})]^T$ with $\hat{\psi}_\sigma(\mathbf{r})$ [$\hat{\psi}_\sigma^\dagger(\mathbf{r})$] being a field operator destroying (creating) a particle located at \mathbf{r} with spin σ ($\sigma = \uparrow, \downarrow$). The anti-commutation or commutation relation $[\hat{\psi}_\sigma(\mathbf{r}), \hat{\psi}_\sigma^\dagger(\mathbf{r}')]_\pm = \delta_{\sigma\sigma'} \delta(\mathbf{r} - \mathbf{r}')$ are required to be respected for fermionic (+) or bosonic operators (-), respectively.

We approximately expand the field operator as

$$\hat{\psi}_\sigma(\mathbf{r}) \approx \sum_{\mathbf{x}, \sigma} W_{\mathbf{x}}(\mathbf{r}) \hat{c}_{\mathbf{x}, \sigma}, \quad (\text{S5})$$

where $\hat{c}_{\mathbf{x},\sigma}$ is the annihilation operator for a particle with spin σ located at the site \mathbf{x} , which satisfies the anti-commutation or commutation relation $[\hat{c}_{\mathbf{x},\sigma}, \hat{c}_{\mathbf{x}',\sigma'}^\dagger]_{\pm} = \delta_{\mathbf{x},\mathbf{x}'}\delta_{\sigma,\sigma'}$ for fermionic (+) or bosonic (−) atoms, respectively, and $W_{\mathbf{x}}(\mathbf{r})$ is the Wannier function for the lowest band of the Hamiltonian with $h_z = V_{SO} = 0$, which is located at the site $\mathbf{x} = \sum_{\nu} j_{\nu} a_{\nu} \mathbf{e}_{\nu}$ with $\nu = x, y, z$.

With the aid of Eq. (S5), we can obtain the following tight-binding Hamiltonian by keeping only the nearest-neighbor hopping terms (see Ref. [S2, S3] for the detailed derivation and verification for its validity),

$$H_{TB} = \sum_{\mathbf{x}} \left[- \sum_{\nu} (J_{\nu} \hat{c}_{\mathbf{x}}^{\dagger} \hat{c}_{\mathbf{x}+a_{\nu}\mathbf{e}_{\nu}} + H.c.) + m_z \hat{c}_{\mathbf{x}}^{\dagger} \sigma_z \hat{c}_{\mathbf{x}} \right] + \sum_{\mathbf{x}} (-1)^{j_x+j_y+j_z} J_{SO} (\hat{c}_{\mathbf{x}}^{\dagger} \sigma_y \hat{c}_{\mathbf{x}+a_x\mathbf{e}_x} - \hat{c}_{\mathbf{x}}^{\dagger} \sigma_x \hat{c}_{\mathbf{x}+a_y\mathbf{e}_y} + H.c.), \quad (\text{S6})$$

where $\hat{c}_{\mathbf{x}}^{\dagger} = (\hat{c}_{\mathbf{x},\uparrow}^{\dagger}, \hat{c}_{\mathbf{x},\downarrow}^{\dagger})$. In the basis of $\Psi(\mathbf{k})^{\dagger} = (e^{-ik_x a_x} \hat{A}_{\mathbf{k}\uparrow}^{\dagger} \ e^{-ik_x a_x} \hat{A}_{\mathbf{k}\downarrow}^{\dagger} \ \hat{B}_{\mathbf{k}\uparrow}^{\dagger} \ \hat{B}_{\mathbf{k}\downarrow}^{\dagger})$ where A and B correspond to two sublattices, the Hamiltonian can be written as in the momentum space $H_{TB} = \sum_{\mathbf{k}} \Psi(\mathbf{k})^{\dagger} H_{3D}(\mathbf{k}) \Psi(\mathbf{k})$, where $H_{3D}(\mathbf{k})$ is the Hamiltonian (5) in the main text. Applying the transformation $\hat{a}_{\mathbf{x}\uparrow} = (-1)^{j_x+j_y+j_z} \hat{c}_{\mathbf{x}\uparrow}$ and $\hat{a}_{\mathbf{x}\downarrow} = \hat{c}_{\mathbf{x}\downarrow}$ reduces the model to the form

$$H'_{TB} = \sum_{\mathbf{x}} [\sum_{\nu} (J_{\nu} \hat{a}_{\mathbf{x}}^{\dagger} \sigma_z \hat{a}_{\mathbf{x}+a_{\nu}\mathbf{e}_{\nu}} + H.c.) + m_z \hat{a}_{\mathbf{x}}^{\dagger} \sigma_z \hat{a}_{\mathbf{x}} - J_{SO} (i \hat{a}_{\mathbf{x}}^{\dagger} \sigma_y \hat{a}_{\mathbf{x}+a_y\mathbf{e}_y} + i \hat{a}_{\mathbf{x}}^{\dagger} \sigma_x \hat{a}_{\mathbf{x}+a_x\mathbf{e}_x} + H.c.)], \quad (\text{S7})$$

where $\hat{a}_{\mathbf{x}}^{\dagger} = (\hat{a}_{\mathbf{x},\uparrow}^{\dagger}, \hat{a}_{\mathbf{x},\downarrow}^{\dagger})$. The lattice structure becomes simple orthorhombic from a rocksalt lattice structure. Using the Fourier transformation, we can write this Hamiltonian in the momentum space as $H'_{TB} = \sum_{\mathbf{k}} \hat{a}_{\mathbf{k}}^{\dagger} H'_{3D}(\mathbf{k}) \hat{a}_{\mathbf{k}}$, where $\hat{a}_{\mathbf{k}}^{\dagger} = (\hat{a}_{\mathbf{k},\uparrow}^{\dagger}, \hat{a}_{\mathbf{k},\downarrow}^{\dagger})$ and $H'_{3D}(\mathbf{k})$ is given in the footnote of the main text.

* yongxuphy@tsinghua.edu.cn

[S1] Y.-B. Yang, L.-M. Duan, and Y. Xu, [arXiv:1801.08255](https://arxiv.org/abs/1801.08255) (2018).

[S2] Y. Xu and C. Zhang, Phys. Rev. A **93**, 063606 (2016).

[S3] Y. Xu and L.-M. Duan, Phys. Rev. A **94**, 053619 (2016).
